Real-time feedback control of 3D Tollmien-Schlichting waves using a dual-slot actuator geometry

SH. S. Vemuri,* R. Bosworth, J. F. Morrison,† and E. C. Kerrigan

Department of Aeronautics, Imperial College London,

South Kensington, London SW7 2AZ, UK

(Dated: April 19, 2018)

Abstract

The growth of Tollmien-Schlichting (TS) waves is experimentally attenuated using a single-input and single-output (SISO) feedback system, where the TS wave packet is generated by a surface point source in a flat-plate boundary layer. The SISO system consists of a single wall-mounted hot wire as the sensor and a miniature speaker as the actuator. The actuation is achieved through a dual-slot geometry to minimise the cavity near-field effects on the sensor. The experimental set-up to generate TS waves or wave packets is very similar to that used by Li and Gaster [1]. The aim is to investigate the performance of the SISO control system in attenuating single-frequency, two-dimensional disturbances generated by these configurations. The necessary plant models are obtained using system identification, the controllers are then designed based on the models and implemented in real-time to test their performance. Cancellation of the rms streamwise velocity fluctuation of TS waves is evident over a significant domain.

* shsvemuri@gmail.com

† j.morrison@imperial.ac.uk

I. INTRODUCTION

Tollmien-Schlichting (TS) waves are naturally occurring instabilities that enter the boundary layer because of the interaction of the wing leading edge with disturbances such as environmental noise, surface imperfections and free-stream vorticity via the receptivity mechanism [2]. In a low free-stream turbulence environment, transition on aircraft wings, especially those with low sweep angles, is initiated by amplification of TS waves. The transition process may be delayed by actively interfering with the linear stage of their growth, which is of obvious importance for wing design.

The idea of controlling TS waves by wave cancellation has been investigated since the 1980s, starting with Milling [3]. The linear nature of the Orr-Sommerfeld equation means that the unstable modes grow independently. Therefore, it should be possible to attenuate the growth of a TS wave by superposing another wave equal in amplitude and 180° out-of-phase. This principle applies to both single-frequency TS waves as well as wave packets. These techniques work by eliminating the growth of perturbations without modification of the mean flow, therefore the energy input is considerably lower than with other active control techniques, such as suction [4], which works on the principle of modifying the mean flow for stabilisation. Previous work [5–9] has tested the superposition concept [3] using various approaches. In summary, the results demonstrate that using superposition it is possible to attenuate wave-like, as well as random, disturbances in an energy-efficient way.

Sturzebecher and Nitsche [10] made the first attempt to attenuate naturally occurring TS wave packets on an unswept wing by an active cancellation scheme in real time. A fast digital processor performing an adaptive control algorithm was used to obtain optimal TS wave packet attenuation. In the first part of that work, a single actuator and two sensors, one upstream (reference sensor) and another downstream (error sensor) were employed. Without any reference to linear stability theory, the transfer function of the controller between the reference sensor and the actuator was continuously adapted to minimise the error signal at the downstream location. This approach was the first published attempt of using the Filtered-X Least Mean Squares (FXLMS) algorithm to attenuate TS waves in real-time. This work resulted in nearly complete cancellation, with TS wave attenuations of about 90% using only a two-dimensional control system. Since the waves could not be completely eliminated, they would grow again and lead to transition. To address this problem, a

streamwise control system consisting of multiple spanwise-arranged panels of sensors and actuators was used, repeated at several downstream locations. Successful cancellation of three-dimensional TS waves was reported.

Zhang [11] tested closed-loop control of TS waves using a Single-Input-Single-Output (SISO) feedback system with a unique dual-slot geometry to minimise the near-field. A fourth-order controller and a complex feedback filter were needed to achieve some reasonable attenuation, because the sensor-actuator distance used was too large. However, despite the high order of the controller, all the frequencies in the TS bandwidth could not be attenuated and an increased end-oscillatory response was reported in the wave packets. Building on this work, the present study uses a similar set-up with a reduced sensor-actuator distance in feedback, as discussed in Section II.

Recently, model-based approaches for adaptive and robust control for attenuation of TS waves have become more popular. Belson *et al.* [12] studied the problem of optimal sensor-actuator placement for robust control of TS waves using DNS data. Bagheri *et al.* [13] showed that it is possible to construct reduced-order models from linearised Navier-Stokes equations for robust feedback control of TS waves using a snapshot-based truncation method. This method was later shown numerically to work in attenuating TS wave packets [14]. Several active control algorithms such as Linear-Quadratic Gaussian (LQG) and FXLMS have been compared [15]: it is concluded that use of LQG or FXLMS significantly out-performs other wave-cancellation techniques. After a significant attenuation of naturally excited TS waves [10], most of the recent experimental developments in active control of TS waves have been centred on attenuating artificially excited TS waves via the FXLMS algorithm using a plasma actuator [16, 17]. All these works reported significant attenuation of artificially excited TS waves, although they require the use of high-energy plasma actuation [18]. While all the model-based approaches compared in [15] are shown to work well numerically, the presence of strong experimental uncertainty suggests that experiments have usually been performed using the adaptive FXLMS algorithm. In their experiments, Fabbiane *et al.* [17] demonstrated the reason for this choice and conclude that FXLMS is simply the most robust algorithm for experiments compared to all the other numerically tested ones: in performance, it is only slightly worse than an optimal LQG control algorithm.

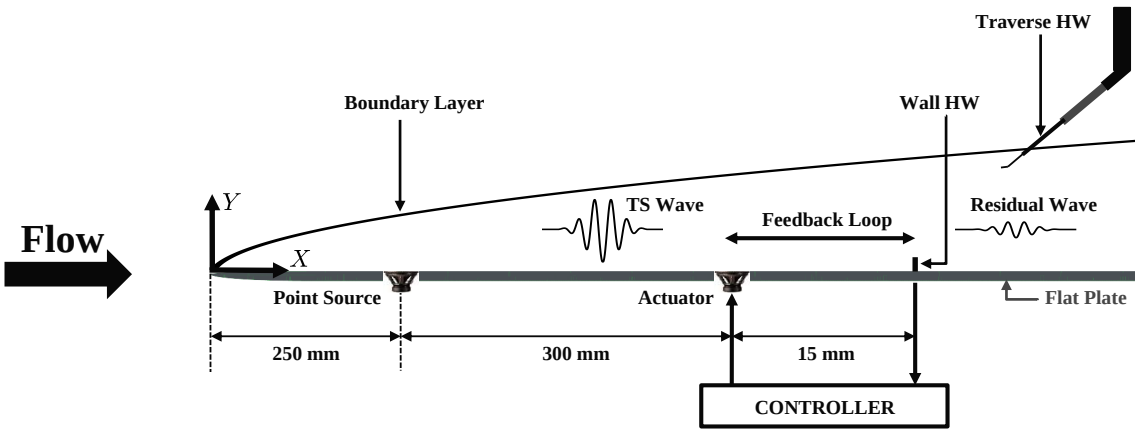

FIG. 1: Schematic of experiment for generating TS waves from a surface point source.

II. EXPERIMENTAL SET-UP

The experiments were carried out in the "3x3" wind tunnel at the Department of Aeronautics, Imperial College, London. The tunnel is of closed-circuit type with a 0.91 m × 0.91 m test section and working length of 4.88 m. The contraction ratio of 9:1 provides a low-disturbance free-stream environment, with axial turbulence intensities of less than 0.05%. Fig. 1 shows the experimental set-up for TS wave-packet generation using a 0.75 mm diameter hole ("point source") and the SISO control system on a flat-plate model. The vertically-mounted, aluminium cast flat plate has an asymmetric modified super-elliptic leading edge, an optimal design based on case A3 [19]; this minimises any disturbance generated by a discontinuity in surface curvature at the termination of the leading edge. A zero pressure gradient along the plate is ensured by the use of a trailing-edge control flap. A speaker (Visaton FRWS 5 SC model) screwed onto the underside of the plate generates puffs of air, perpendicular to the plate into the boundary layer. The speaker is carefully sealed to avoid any unwanted leakage of air from the non-measurement side. The SISO configuration is similar to that used by Zhang [20], but with a much smaller sensor-actuator distance. A wall-mounted hot wire (manufactured in-house based on Dantec 55P01 design) downstream of the actuator provides the difference of streamwise velocity on which the control is based. Positioning of the control sensor in the near-field of the actuator has to be avoided because the initial disturbance that gives rise to the TS wave packet is strongest along the centre-line and decays with distance along the span: this near field is not to be modelled. For this reason, a 3 mm region in between a single 12 mm long, 0.75 mm wide slot was blocked, resulting

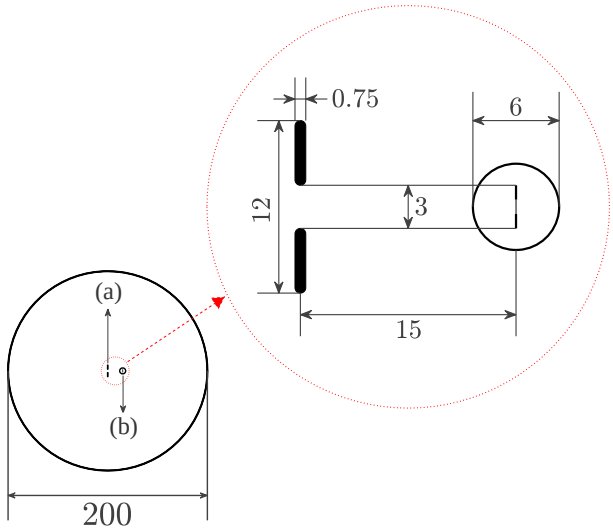

FIG. 2: Schematic of the control components mounted on a removable disc: (a) the dual actuator slots; (b) the wall-mounted hot-wire sensor. All dimensions shown in the close-up view are in mm. The hot wire protrudes above the plate surface by about 0.5 mm.

in an actuator geometry of two identical 4.5 mm long slots across the span. Fig. 2 shows the schematic of the control system mounted on a 200 mm removable disc flush-mounted in the flat plate centred at $X = 550$ mm (where X is measured from the leading edge of the plate). The figure shows how the wall-mounted hot wire is positioned immediately downstream of the intervening gap. The actuator operates approximately 300 mm downstream of the source. The feedback loop between the wall-mounted hot wire (which is a further 15 mm downstream) and the actuator provides the control. Fig. 3 shows a photograph of the actuator, the surface hot wire and the traverse hot wire used for downstream measurements.

The governing Orr-Sommerfeld equation is fourth-order in space but could be several orders higher in time. Hence, there is no direct way in which a numerical model may be obtained for control. The block diagram for the present control approach is shown in Fig. 4. The closed-loop transfer function is given by

$$G(s) = \frac{FG_d}{(1 + KG_aF)}, \tag{1}$$

where F is the filter, G_d is the transfer function between the point source and the wall sensor, and G_a is that between the actuator and the wall sensor. The delay introduced by the filter alone is expected to be negligible compared to the TS-wave convection delay. For experimental purposes, the filter transfer function F is usually grouped with the transfer

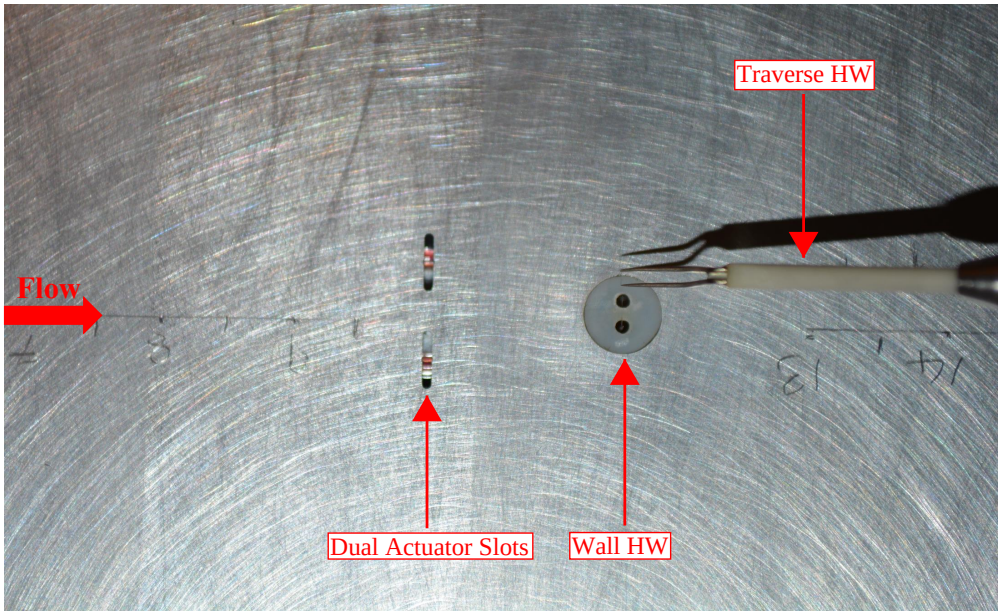

FIG. 3: Picture showing a close-up view of the dual actuator slot geometry and the wall hot wire used in control experiments. The traverse hot wire is aligned with the wall hot wire before performing boundary layer measurements downstream of the control system.

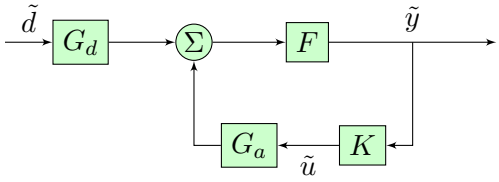

FIG. 4: Feedback control block diagram: G_d is transfer function between the point source and the wall sensor; G_a is the transfer function between the actuator and the wall sensor; the controller is K and the filter F.

functions G_d and G_a. This approach is economical, since it eliminates the necessity of estimating the filter transfer function separately, regardless of the type of excitation used. The grouped product of transfer functions, i.e. (FG_d) and (FG_a), is obtained by classical frequency-sweep techniques with an emphasis around the TS bandwidth, which, in turn, is calculated from the branch points of the neutral stability curve for the experimental conditions. Here, we simply use G_d and G_a to denote the grouped transfer functions FG_d and FG_a, respectively. A Nyquist stability plot is used to optimise the controller gain in closed loop while still ensuring stability. Control performance is evaluated downstream through boundary-layer traverses with a hot wire (Dantec 55P05 model). The output signals

from both the traverse and the wall-mounted hot wires are passed through a 1 Hz–5 kHz analog band-pass filter (Krohn-Hite 3384 model) before being digitised using DAQ units at a sample rate of 10 kHz. The raw signals from both the hot wires are acquired on separate input channels on the main DAQ unit (NI USB-6229 BNC). All the experiments are carried out at a free-stream velocity U_∞ of 12 ms^{-1}. Only single hot wires for measurement of the axial velocity are used.

The controller design is based on experimentally determined frequency response data (FRD) models G_d and G_a. The controller transfer functions are discretised using a Zero-Order Hold (ZOH) and implemented digitally in real time using the National Instruments PXIe-1078 chassis. The PXI system has a Real-Time Operating System (RTOS) and a DAQ card (NI DAQ BNC 2110 model). The filtered fluctuating part of the wall hot-wire signal u' is fed as the input to the PXI via the DAQ card. Convolution of this input signal with the discretised transfer function for the controller provides the actuator output signal. This operation is performed continuously in real time on the PXI chassis. The output signal obtained from the DAQ card is sent directly to the power amplifier that drives the speaker used for actuation. The entire closed loop, as a result, operates at a frequency of 10 kHz.

In addition to the above operations, input and output data from the PXI system is continuously streamed back to the main terminal via a separate ethernet card. The signal for exciting the point source is always performed on the main terminal via the main DAQ (NI USB 6229 BNC). A power amplifier (YAMAHA XM4080 model) is used to amplify the gain levels before sending signals to both the source and the actuator since the DAQ unit alone cannot provide sufficient current to drive the speakers directly.

III. BASE FLOW CHARACTERISATION AND DISTURBANCE GENERATION

Initial experiments are carried out to ensure Blasius flow conditions. The incidence of the trailing edge flap is adjusted using three support mounts holding the test plate. Fig. 5 shows scaled boundary layer profiles measured at 20 streamwise stations and compared to Blasius theory. The shape factors measured are less than 2% of the theoretical value 2.5914 at all the stations, with a mean value 2.5983 and standard deviation 0.017.

It is well known that the characteristics of a Linear Time Invariant (LTI) system can be completely obtained by studying its impulse response. The output of such a system to any

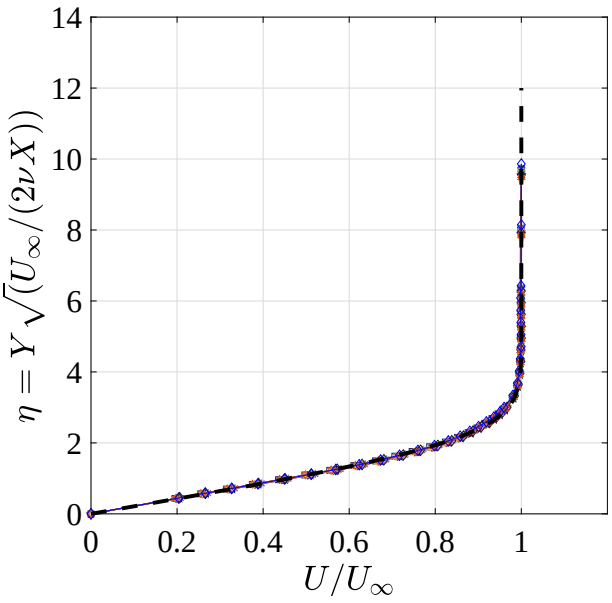

FIG. 5: Experimental boundary layer profiles scaled and compared to the Blasius boundary layer at $X = 445$ to 635 mm. The black dashed line shows the Blasius profile.

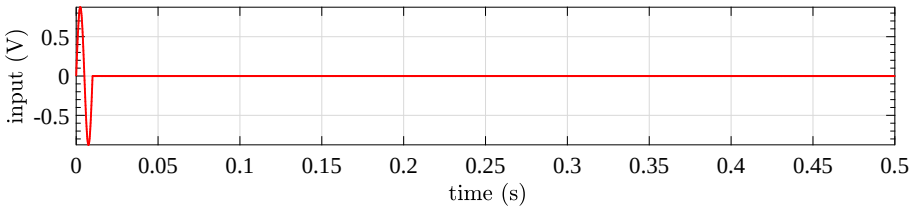

FIG. 6: Impulse input for generating TS wave packets in the boundary layer.

given input can be obtained by convolving the input signal with the impulse response of the system. Impulse inputs to the point source result in travelling TS wave packets in the boundary layer. In the experiment, the pulse itself lasts for 10 msec and each sample is 0.5 sec long, as shown in Fig. 6. 200 such samples acquired by the hot wire are used to obtain an ensemble average of the wave packet at each traverse point in the boundary layer.

The resulting wave packet in the boundary layer for one test case is shown in Fig. 7. An impulse input excites all the frequencies, only a certain narrow band of which result in growing TS waves. At a given location in the boundary layer, the TS wave packet takes its form because of the combination of these growing frequencies among all others excited.

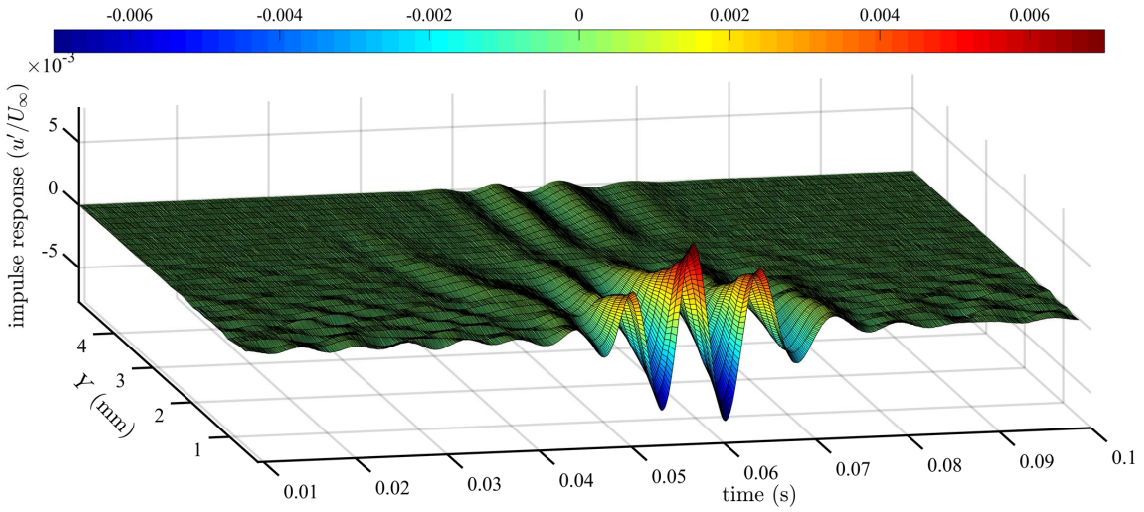

FIG. 7: Time history of the normalised streamwise velocity fluctuations through the entire boundary layer, at $X = 500$ mm for an impulse excitation of the point source.

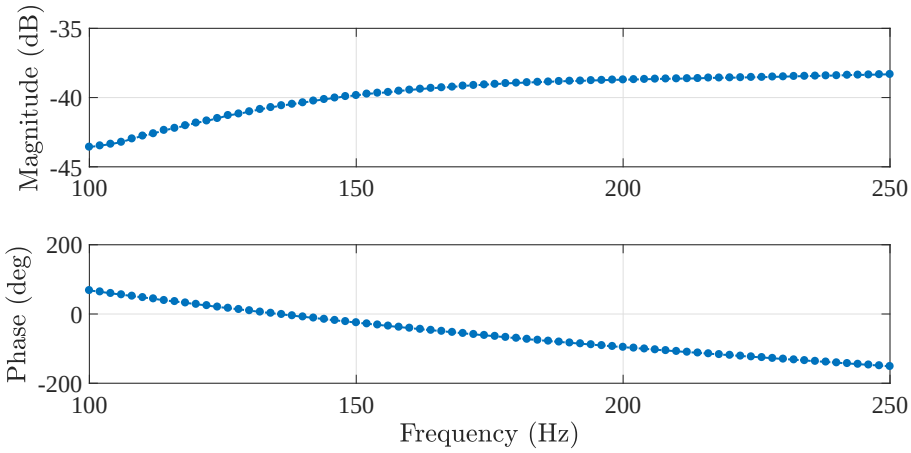

FIG. 8: Bode plot of the FRD model G_a.

IV. CONTROLLER DESIGN

The frequency response data (FRD) models of the system, G_a and G_d, were obtained by acquiring data simultaneously for 36 seconds, with a sinusoidal input voltage of the point source, and the filtered output voltage from wall-mounted hot wire at each frequency in the sweep. A Blackman-Tukey approach [21] was used to obtain the Bode plots from the input-output data. The Bode plot of the FRD model G_a is shown in Fig. 8. The Bode plot of the FRD model, G_d, is shown in Fig. 9. Frequency sweeps were performed from 100 Hz to 250 Hz in steps of 2 Hz for the model G_d, with and without control. The peak in magnitude of G_d without control (red) is obtained at 156 Hz. The controller attenuated each frequency

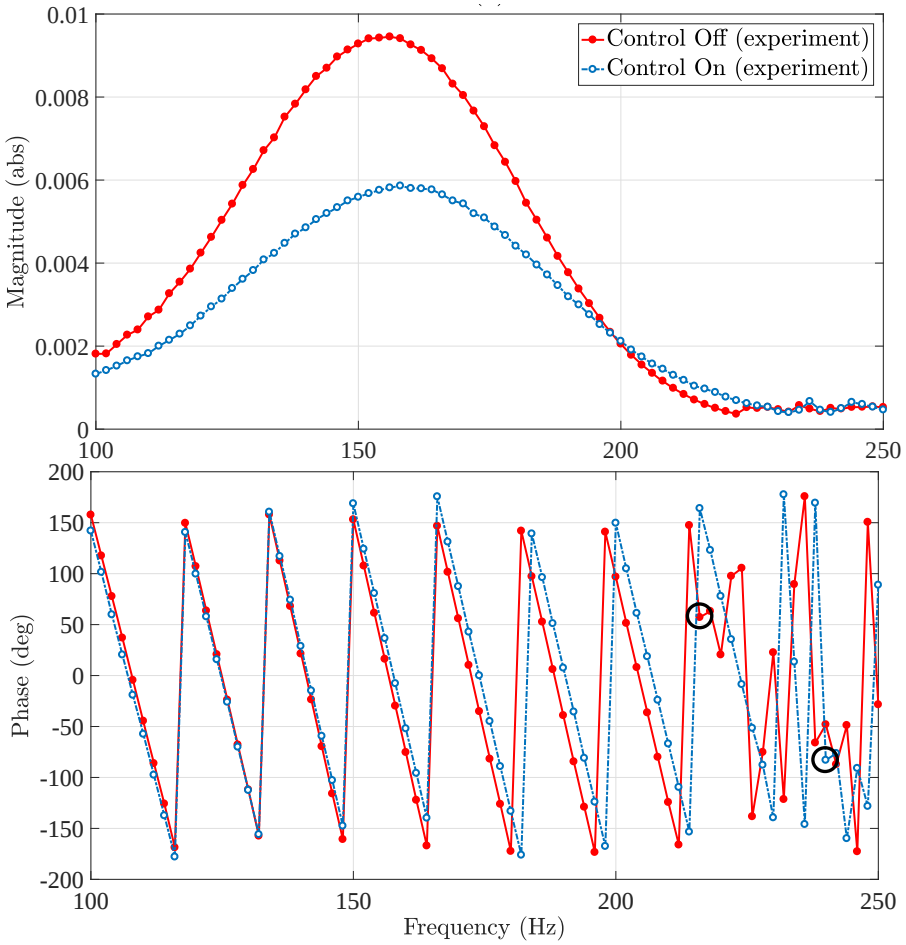

FIG. 9: Bode plot showing performance of the controller in experiment with point source. The break points in phase are circled in black.

in the bandwidth 100 to 200 Hz. A maximum attenuation of 40% in u'_{rms} (4.53 dB) was obtained at 140 Hz. The phase (wrapped to $\pm 180°$) in the Bode plot looks like a set of nearly parallel straight lines, a characteristic of a system with delay. In this case, the delay is expected because of the finite convection time associated with the wave travelling from the point source to the wall hot wire. The phase plot of G_d exhibits a steeper variation when wrapped to $\pm 180°$ compared to G_a, because of longer convection delay.

Controllers up to second order have been tested, but increasing the order of the controller did not improve the performance noticeably [22]. Therefore, only the results for proportional control are shown in this paper. It will be shown elsewhere that proportional control alone provides attenuation of TS waves [22]. The controller K was implemented in real-time based on the proportional output feedback gain, where $K = -60$. Fig. 10 shows the Nyquist plot

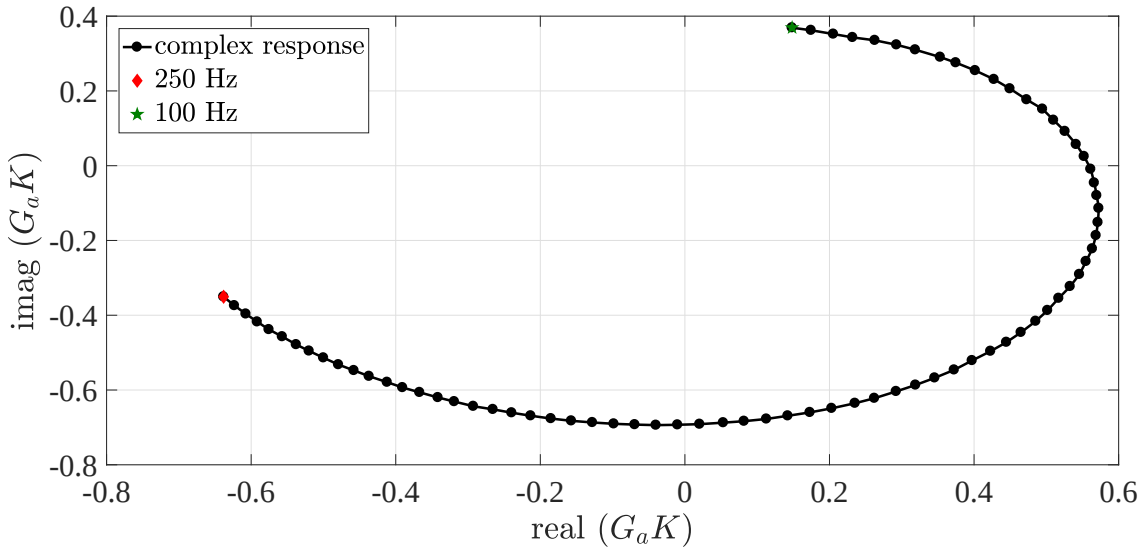

FIG. 10: Nyquist plot of the loop gain in the feedback control of TS waves generated from a point source. The first and the last frequencies are shown to indicate the sense of direction.

of the loop gain (G_aK), which ensures stability of the closed loop since the plot does not encircle the -1 point in the frequency range tested.

As the frequency is increased, the TS wave amplitude continues to decrease until there comes a point when the amplitude is so small that the signal shown by the hot wire no longer has a clear sine wave form. This frequency marks the end of the TS wave bandwidth. Excitations with frequencies higher than this do not generate TS waves, so the hot wire shows only the natural fluctuations in the boundary layer. This point can be identified in a frequency sweep analysis by checking for break points defined by deviation of the wrapped phase structure of the Bode plot. At the break point, the wrapped phase plot breaks from its characteristic 'nearly parallel lines' structure. The break point in phase is approximately the frequency that marks the end of TS bandwidth for the chosen experimental conditions. These are shown circled in black in Fig. 9 in both the frequency sweeps (with and without control). Without control, the break point in phase is obtained at 216 Hz, and with control it shifts slightly to 240 Hz. This is because the controller is energising the tiny bandwidth towards the end of the sweep. A small amplification region in magnitude can also be noted from approximately 200 Hz to 240 Hz, before the response becomes insignificant. However, this amplification is negligible compared to the attenuation achieved over the entire bandwidth. In addition, these higher frequencies decay naturally downstream because they have positive

imaginary parts in their eigenvalues. This is confirmed by boundary layer measurements downstream of the control system.

V. BOUNDARY LAYER RESPONSE

All the measurements shown so far were performed at the wall hot-wire location. To investigate the controller performance more fully, boundary layer scans are performed on a 16×6 grid of streamwise locations, X = 575 (25) 950 mm and spanwise locations, Z = 0 (10) 50 mm, where X is the distance from the leading edge and Z is the spanwise distance from the centre line. For a clearer picture of the influence of the dual-slot actuator, the data are assumed to be symmetrical about the centre line and, for presentational purposes, mirrored about it. The most attenuated frequency, 140 Hz, is chosen for excitation of TS waves in these measurements.

The boundary layer measurements in this grid were performed twice, first without control and second, with control. For accurate positioning of the traverse hot wire, it is first aligned with the wall hot wire before starting the run (see Fig. 3). A full streamwise run was performed covering all the X-locations, before moving to another spanwise position to repeat the procedure. Movement of the traverse was always performed in the same direction to ensure that any backlash was removed. The frequency at which control produced the greatest attentuation, 140 Hz, was also used to excite single frequency TS waves from the point source. Each of the 34 points in the boundary layer were sampled for 11 seconds.

The integral TS wave amplitude ($A_{TS,int}$) at each streamwise location is obtained by integrating the area under the double hump (rms amplitude) profile:

$$A_{TS,int} = \int_0^{y_{max}} u'_{rms} dy, \tag{2}$$

where y_{max} is the distance from the wall to the last measurement point, outside the edge of the boundary layer, determined by the change in mean velocity being less than 0.5% of the free-stream value. The integral is obtained via the trapezoidal method with spacing defined by the step sizes used in the boundary layer measurement. Thus the step sizes at each point in the integration domain are the same for both controlled and uncontrolled flows.

A cancellation map is shown in Fig. 11 based on the integrated values of u'_{rms} at each point in the grid. As can be seen, a finite distance (about 100 mm) is required for the

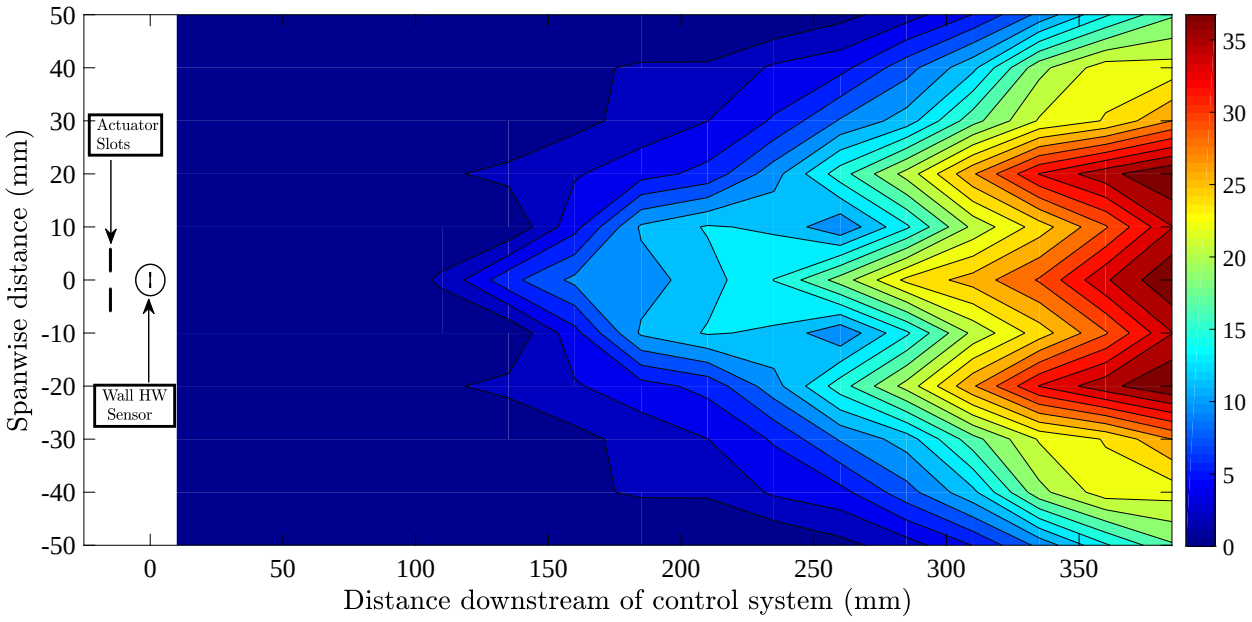

FIG. 11: Cancellation percentage map: $A_{TS,int}$. Colourbar shows cancellation due to control %. Figure also shows the location of the actuator dual slots and the wall hot wire. The flow direction is from left to right.

cancellation to be effective. This finding is in line with results in [20]. Cancellation increases with downsteam distance. The small amplification seen in the Bode plot (Fig. 9) from 200 Hz to 240 Hz after control appears to have no influence: these modes have small amplitudes and decay naturally after a short distance downstream.

The effect of the dual-slot actuator geometry can also be seen in the cancellation map. Each slot behaves like a source and therefore has its own independent wedges. These wedges initially grow independently, meet at some distance downstream, and grow into a stronger, wider wedge. In this case, since these slots are used for actuation, a progressive attenuation is therefore realised along their combined wedge. A maximum cancellation of about 39% in u'_{rms} is achieved along the centreline at $X = 950$ mm. This corresponds to approximately a 63% reduction in rms energy. This cancellation is a significant improvement from [20], who reported a maximum attenuation of 30% in u'_{rms} (50% reduction in energy) using a fourth-order controller. This improvement can be attributed to the smaller sensor-actuator distance used here.

The spanwise amplitude distribution with and without control at $X = 950$ is shown in Fig. 12. As expected, the maximum growth in u'_{rms} is obtained along the centre line and this

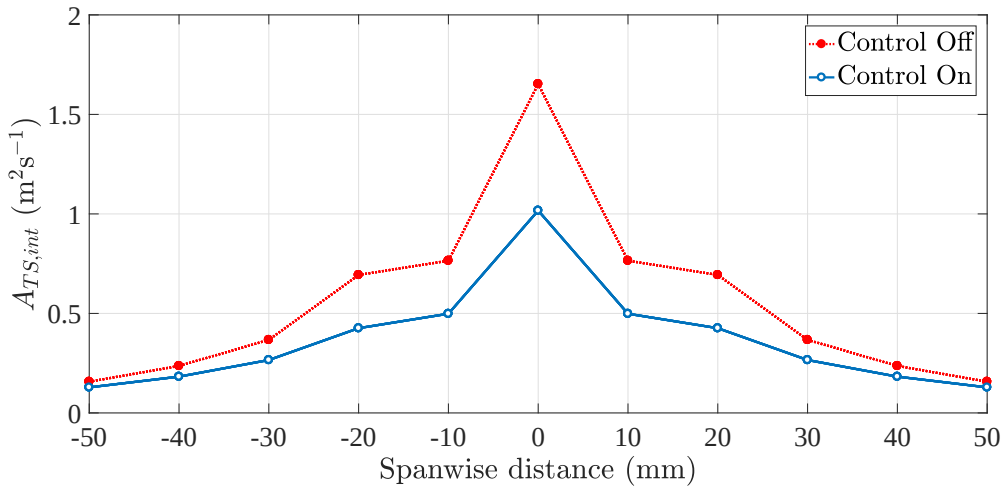

FIG. 12: Spanwise distribution of the integrated u'_{rms} at 385 mm downstream of the wall hot wire (X = 950 mm), with and without control.

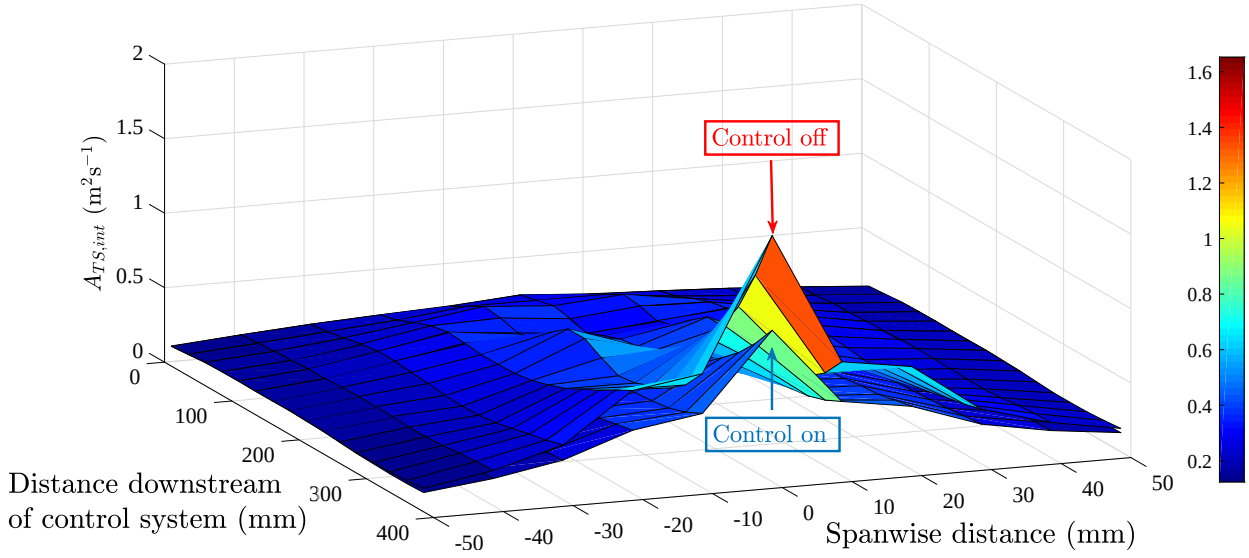

FIG. 13: A surface plot of the spanwise distribution of the integrated u'_{rms} at all the streamwise locations in the measurement grid, with and without control.

diminishes towards either side. The individual wedges from the actuator slots also merge well ahead of this streamwise location, and this is the last X-point in the measurement grid. Consequently, the maximum attenuation, 39 % in u'_{rms} is achieved at this point. Fig. 13 shows a combined plot using all streamwise locations in the grid to form a surface plot.

From linear stability theory, the growth of TS wave amplitude $A_{TS,int}$ is expected to be exponential when plotted on a linear axes as shown in Fig. 14(a). With the same data

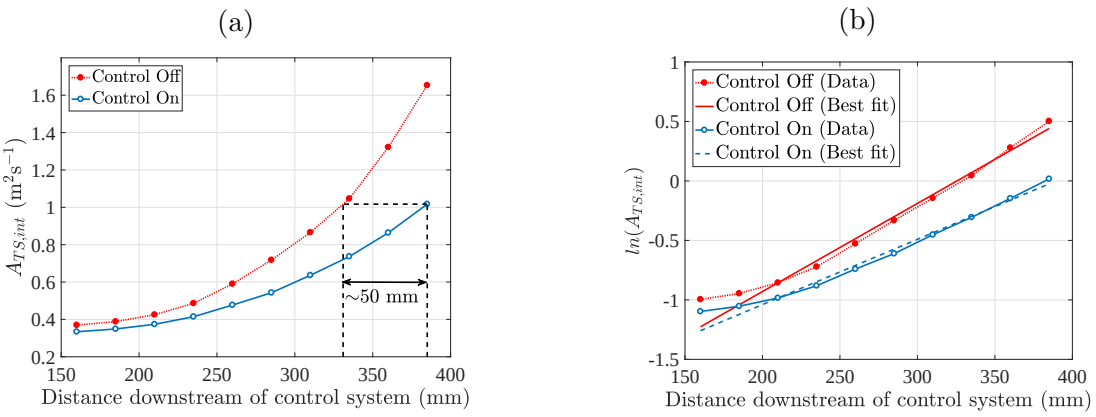

FIG. 14: Growth of the integrated u'_{rms} profiles plotted at various streamwise locations along the centreline, inside the control wedge shown in the cancellation percentage map: (a) Linear plot (b) Semi-log plot. The data are fitted with best fit straight lines on the semi-log plot.

plotted on a semi-log axis, the variation is expected to be linear, Fig. 14(b). At the last measurement point ($X = 950$ mm), with control on, TS wave amplitudes reached a value that occurred 50 mm upstream without control. The corresponding change in N-factor due to control is approximately 0.49.

The semi-log plots shown further serve as a test to check the assumption that the TS wave growth is linear in the control domain and to characterise the control effect on the growth rate α_i. As can be seen from Fig. 14(b), the growth rates on the semi-log plot in both cases vary in almost a linear fashion with streamwise distance, which confirms exponential growth.

VI. DISCUSSION AND CONCLUSIONS

In the present study, real-time feedback control has been successfully implemented on 3D TS waves generated from a surface point source. A SISO control system was used, consisting of a single wall-mounted hot-wire sensor and two adjacent slots, which act as an actuating source.

Measurements using the wall-mounted hot wire of the feedback control system show that, in single-frequency TS wave excitations, a significant cancellation is obtained for almost all the frequencies in the TS wave bandwidth. The attenuation achieved by the control system is established by performing full boundary-layer scans in a 16×6 grid of streamwise and

spanwise locations downstream of the control system for a 140 Hz TS wave from the point source. Measurements in this grid show that the attenuation from the dual slot actuation takes effect about 100 mm downstream. Further downstream, the attenuation becomes more marked and spreads to a wider region across the span, as the individual contributions in wedge-shaped regions from both the actuator slots merge. The cancellation of the rms streamwise velocity fluctuation is evident over a significant domain. A maximum attenuation of about 39% in u'_{rms} (63% in energy) is achieved along the centreline at $X = 950$ mm. With control on, the TS waves reach an amplitude which occurred 50 mm further upstream in the control off case at the last measurement location ($X = 950$ mm). This corresponds to a change in N-factor of 0.49.

VII. ACKNOWLEDGEMENTS

We thank Professor Mike Gaster for use of his stability codes and many valuable suggestions. We are indebted to Airbus (contract no. IW202838) and EPSRC (LFC-UK Programme Grant no. EP/I037946) for financial support.

[1] Y. Li and M. Gaster, "Active control of boundary-layer instabilities," J. Fluid Mech. **550**, 185–205 (2006).

[2] W. S. Saric, H. L. Reed, and E. J. Kerschen, "Boundary-layer receptivity to freestream disturbances," Annu. Rev. Fluid Mech. **34**, 291–319 (2002).

[3] R. W. Milling, "Tollmien–Schlichting wave cancellation," Phys. Fluids **24**, 979 (1981).

[4] M. Engert and W. Nitsche, "Active cancellation of Tollmien-Schlichting instabilities up to $M = 0.40$," 26th Intl Cong. Aero. Sci. (2008).

[5] H. W. Liepmann, G. L. Brown, and D. M. Nosenchuck, "Control of laminar-instability waves using a new technique," J. Fluid Mech. **118**, 187–200 (1982).

[6] H. W. Liepmann and D. M. Nosenchuck, "On active control of laminar-turbulent transition on two-dimensional wings," J. Fluid Mech. **118**, 201–204 (1982).

[7] A. S. W. Thomas, "The control of boundary-layer transition using a wave-superposition principle," J. Fluid Mech. **137**, 233–250 (1983).

[8] P. Pupator and W. Saric, "Control of Random Disturbances in a Boundary Layer," AIAA Paper , 89–107 (1988).

[9] D. M. Ladd, "Control of Natural Laminar Instability Waves on an Axisymmetric Body," AIAA Paper **28**, 367–369 (1990).

[10] D. Sturzebecher and W. Nitsche, "Active cancellation of Tollmien–Schlichting instabilities on a wing using multi-channel sensor actuator systems," Intl J. Heat Fluid Flow **24**, 572–583 (2003).

[11] Z. Zhang, *Closed-Loop Flow Control for Boundary Layer Instabilities*, Ph.D. thesis, Queen Mary, University of London (2008).

[12] B. A. Belson, O. Semeraro, C. W. Rowley, and D. S. Henningson, "Feedback control of instabilities in the two-dimensional Blasius boundary layer: The role of sensors and actuators," Phys. Fluids **25**, 054106 (2013).

[13] S. Bagheri, L. Brandt, and D. S. Henningson, "Input-output analysis, model reduction and control of the flat-plate boundary layer," J. Fluid Mech. **620**, 263–298 (2009).

[14] O. Semeraro, S. Bagheri, L. Brandt, and D. S. Henningson, "Feedback control of three-dimensional optimal disturbances using reduced-order models," J. Fluid Mech. **677**, 63–102 (2011).

[15] N. Fabbiane, O. Semeraro, S. Bagheri, and D. S. Henningson, "Adaptive and model-based control theory applied to convectively unstable flows," Appl. Mech. Rev. **66**, 060801 (2014).

[16] B Simon, T Nemitz, J Rohlfing, F Fischer, D Mayer, and S Grundmann, "Active flow control of laminar boundary layers for variable flow conditions," Intl J. Heat Fluid Flow **56**, 344–354 (2015).

[17] N. Fabbiane, B. Simon, F. Fischer, S. Grundmann, S. Bagheri, and D. S. Henningson, "On the role of adaptivity for robust laminar flow control," J. Fluid Mech. **767**, 1–12 (2015).

[18] N. Fabbiane, S. Bagheri, and D. S. Henningson, "Energy efficiency and performance limitations of linear adaptive control for transition delay," J. Fluid Mech. **810**, 60–81 (2017).

[19] R. E. Hanson, H. P. Buckley, and P. Lavoie, "Aerodynamic optimization of the flat-plate leading edge for experimental studies of laminar and transitional boundary layers," Exp. Fluids **53**, 863–871 (2012).

[20] Z. Zhang, "Experiments of closed-loop flow control for laminar boundary layers," Int. J. of Mod. Phy: Conf. Series **19**, 242–249 (2012).

[21] L. Ljung, *System Identification* (Springer, 1998).

[22] SH. S. Vemuri, *Active Control of Tollmien-Schlichting Waves in a Blasius Boundary Layer*, Ph.D. thesis, Imperial College London (2017).